RSC Advances

PAPER

View Article Online
View Journal | View Issue

Cite this: *RSC Adv.*, 2017, **7**, 33263

A novel hexahydroquinazolin-2-amine-based fluorescence sensor for Cu^{2+} from isolongifolanone and its biological applications†

Zhonglong Wang,[a] Jinlai Yang,[b] Yiqin Yang,[c] Hua Fang,[d] Xu Xu,[ae] Jian Rui,[a] Fan Su,[a] Haijun Xu[ae] and Shifa Wang *[ae]

Received 21st April 2017
Accepted 7th June 2017

DOI: 10.1039/c7ra04484d

rsc.li/rsc-advances

Pyrimidine-based derivatives **2a–2c** were synthesized from renewable isolongifolanone, and compound **2c** exhibited high selectivity and sensitivity toward Cu^{2+} ions with a low detection limit of 4×10^{-8} M, a wide pH range (5–11), and a short response time (30 s). The sensor still retained good fluorescence selectivity to Cu^{2+} ions when applied to fluorescence imaging in living black mice. Therefore, compound **2c** can be used as an effective fluorescence probe and imaging agent for detecting Cu^{2+} ions.

Introduction

In recent years, selective chemo-sensors for recognizing specific metal ions have attracted more and more research interests. In particular, there have been advances in the development of sensors for detecting and tracking transition metal ions, such as Cu^{2+}, Fe^{3+}, Cr^{3+}, and Cd^{2+}, which are important in chemical and biological science, and the excellent properties of these sensors make them capable of being used as an efficient way to protect the environment.[1–9] Copper is an essential trace element and exists in the form of copper protein in the human body. Furthermore, copper mainly acts as biocatalyst in the human body and plays a pivotal role in hematopoiesis, angiomalacia, metabolism and hormone secretion.[10] In spite of these good biological functions, excessive levels of copper can result in many kinds of diseases such as Menkes or Wilson disease,[11] Alzheimer's disease,[12–14] and prion disease.[15] Copper can be ingested from polluted water and foods. Thus, the detection of copper ions in the environment and *in vivo* is important for human health.

A fluorescence probe is a simple, fast, and sensitive way of detecting copper ions compared with traditional methods such as electrochemistry,[16] spectrophotometry,[17] voltammetry,[18] and atomic absorption spectroscopy.[19] Many sensitive fluorescence probes for Cu^{2+} have been reported, such as ferrocenyl,[20] benzimidazole,[21] benzothiazole,[22,23] pyrene,[24,25] BODIPY,[26,27] rhodamine,[28–31] *etc.* Pyrimidine is a typical nitrogen heterocyclic compound and has many structure sites that can be modified. Pyrimidine has been widely used in the fields of pesticides[32] and medicine in the past few years,[33,34] but there are few reports on its use in fluorescence probes. Due to the nitrogen heterocycle, pyrimidine derivatives can bind metal ions to serve as a potential probe.

Isolongifolanone is prepared from natural longifolene by oxidation,[35,36] and it can serve as a renewable terpenoid material to synthesize various derivatives such as α,β-unsaturated ketones, pyrazole, and pyrimidine; these derivatives have been used in the fields of anophelifuges and antineoplastics.[37] However, there is no reported derivative that has been used for detecting metal ions and other substances as a florescence probe. In addition, longifolene is a main component of natural turpentine with great biological compatibility. Therefore, longifolene derivatives have good cell membrane permeability. This excellent cell membrane permeability enables the derivatives to be used for bio-imaging in organisms. In view of the above-mentioned merits, we believe that we can design some useful compounds as probes based on isolongifolanone.

In this study, we synthesized three pyrimidine-based derivatives **2a–2c** from isolongifolanone and investigated whether the fluorescence properties were affected by the locations of pyridine. After that, compound **2c** was selected as a moderate florescence probe from the three compounds. Compound **2c** showed obvious fluorescence quenching with the addition of Cu^{2+} ions. The optical properties of compound **2c** towards Cu^{2+} ions have been investigated using various instruments and

[a]College of Chemical Engineering, Nanjing Forestry University, Nanjing, Jiangsu 210037, People's Republic of China. E-mail: wangshifa65@163.com; Fax: +86 25 85427812; Tel: +86 25 85427812

[b]Key Laboratory of High Efficient Processing of Bamboo of Zhejiang Province, China National Bamboo Research Center, Hangzhou 310012, Zhejiang, China

[c]Institute of Light Industry Science and Engineering, Nanjing Forestry University, Nanjing, Jiangsu 210037, People's Republic of China

[d]Department of Chemistry and Material Science, College of Science, Nanjing Forestry University, Nanjing, Jiangsu 210037, People's Republic of China

[e]Jiangsu Key Lab of Biomass-Based Green Fuels and Chemicals, Nanjing 210037, People's Republic of China

† Electronic supplementary information (ESI) available. CCDC 1535362. For ESI and crystallographic data in CIF or other electronic format see DOI: 10.1039/c7ra04484d

means, and in addition, compound **2c** has been successfully applied to the identification of Cu^{2+} ions *in vivo* in black mice.

Results and discussion

Synthesis

The synthetic route of compounds **2a–2c** is shown in Scheme 1. Compounds **1a–1c** were first synthesized by the aldol condensation reaction of isolongifolanone and pyridinecarboxaldehyde, and then compounds **2a–2c** were synthesized by a reaction of compound **1a** (**1b** or **1c**) and guanidine hydrochloride in the presence of potassium *tert*-butylate in *tert*-butyl alcohol. The synthesized compounds **2a–2c** were characterized by IR, NMR and HRMS techniques. Moreover, compound **2c** was characterized by single-crystal X-ray diffraction (Table S1, ESI† and Fig. 1). These analyses confirmed **2c** to be 6,6,10,10-tetramethyl-4-(pyridine-4′-yl)-5,7,8,9,10,10*a*-hexahydro-6*H*-6*a*,9-methanobenzo[*h*]quinazolin-2-amine.

UV-vis and fluorescence properties in solution

In order to investigate the fluorescence properties of the three compounds (**2a–2c**) in the solution state, the compounds were separately dissolved in 8/2 (v/v) ethanol–water solution (1×10^{-4} M). The compounds (**2a–2c**) appeared as colourless and transparent solutions under sunlight (Fig. S1a†), while the compounds (**2a–2c**) could emit fluorescence under 365 nm UV light. Compounds **2a** and **2c** emitted strong blue light, but compound **2b** emitted weaker light under UV light (Fig. S1b†), therefore the locations of the pyridine substituents have an influence on the fluorescence properties in solution. Compared to the insignificant colour change of compounds **2b** and **2c** with the addition of 1.5 mM copper ions, the colour of compound **2a** changed from colourless to pale yellow under sunlight (Fig. S1c†); this may indicate that the coordinating ability of compound **2a** with Cu^{2+} ions was superior to that of compounds **2b** and **2c**. Compounds **2a–2c** quench fluorescence in the presence of Cu^{2+} ions under 365 nm UV light, but only compound **2b** showed a faint quenching change due to its own weak fluorescence (Fig. S1d†). We concluded that compounds

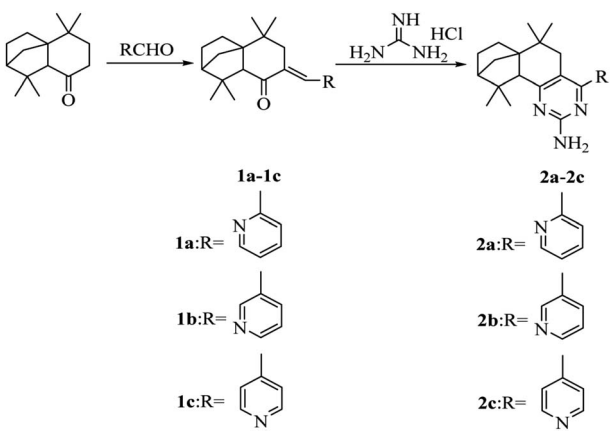

Scheme 1 Synthesis of compounds **2a–2c**.

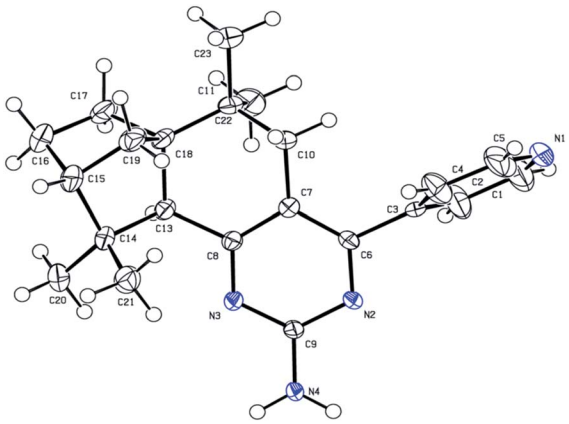

Fig. 1 X-ray crystal structure of compound **2c**.

2a and **2c** could serve as fluorescence probes for detecting Cu^{2+} ions, so compound **2c** was selected as a moderate sample to study its optical properties.

Compound **2c** in the liquid state (1×10^{-5} M) emitted bright blue light when it was dissolved in different organic solvents such as ethanol, methanol, acetonitrile, ethyl acetate, and dichloromethane. The sunlight and fluorescence responses of compound **2c** were further investigated with the addition of 150 μM of various metal ions such as Zn^{2+}, Hg^{2+}, Fe^{2+}, Fe^{3+}, Cu^{2+}, Cr^{3+}, Co^{2+}, La^{3+}, Ag^{+}, Al^{3+}, and Pb^{2+} in ethanol–water media (v/v = 8/2, pH = 7.2). The solutions of compound **2c** maintained their original colours in the presence of metal ions under sunlight (Fig. 2a). However, the solution changed from bright blue to colourless after the addition of Cu^{2+} under 365 nm UV light (Fig. 2b). Meanwhile, the addition of the other metal ions did not lead to fluorescence quenching. Thus, the results showed that the new compound could be used as a novel fluorescence sensor for identifying copper ions.

The UV-visible spectrum of compound **2c** (1×10^{-4} M) was measured in 8/2 (v/v) ethanol–water solution (20 mM HEPES, pH = 7.2). It had two main absorption peaks; the narrow band was strong at 225 nm and the broad band at 325 nm was very

Fig. 2 Photographs of compound **2c** (1×10^{-5} M) with the addition of various metal ions (1.5×10^{-4} M) in CH_3CH_2OH–H_2O (v/v = 8/2, 20 mM HEPES buffer, pH = 7.2) solution under sunlight (a) and 365 nm UV light (b).

weak (Fig. S2†). The complexing interaction of compound **2c** with metal ions (1 mM) such as Zn^{2+}, Hg^{2+}, Fe^{2+}, Fe^{3+}, Cu^{2+}, Cr^{3+}, Co^{2+}, La^{3+}, Ag^{+}, Al^{3+}, and Pb^{2+} was observed using UV-vis spectroscopy. The results showed that the absorbance of compound **2c** at 225 nm obviously increased with the addition of La^{3+}, Ag^{+}, Co^{2+}, and Pb^{2+} and the weak band in the range 280–325 nm became more intense in the case of Cu^{2+} ions.

To investigate the binding properties of compound **2c** with Cu^{2+} ions, we measured the UV-vis absorption spectra of compound **2c** (1×10^{-4} M) with the addition of various amounts of Cu^{2+} ions (0–1.6×10^{-3} M) in 8/2 (v/v) ethanol–water solution (20 mM HEPES, pH = 7.2). As shown in Fig. S3,† with increasing concentrations of Cu^{2+} ions (0–1.6×10^{-3} M), the UV-vis absorption spectra of compound **2c** show a gradually enhanced intensity at 325 nm, whereas another absorption peak at 225 nm had no obvious change with the increasing concentrations of Cu^{2+} ions. It is possible that the complexation of compound **2c** with Cu^{2+} ions led to this tendency of the absorption peak.

Next, the selectivity of compound **2c** (1×10^{-5} M) was also evaluated after adding 10 equivalents of different metal ions using a fluorescence spectrophotometer (Fig. 3a and b). All the salts of the Pb^{2+}, Ag^{+}, Al^{3+}, Co^{2+}, Cr^{3+}, Fe^{3+}, Hg^{2+}, La^{3+}, Zn^{2+}, Fe^{2+}, and Cu^{2+} ions and compound **2c** were dissolved in 8/2 (v/v) ethanol–water solution (20 mM HEPES, pH = 7.2). A slight fluorescence enhancement occurred with the addition of La^{3+}, Al^{3+}, and Ag^{+}, while the addition of Co^{2+}, Cr^{3+}, Fe^{3+}, Hg^{2+}, Zn^{2+}, and Fe^{2+} into the solution of compound **2c** led to a tiny fluorescence decrease. Compound **2c** only displayed sharp fluorescence quenching after the addition of Cu^{2+} ions. Compared to Cu^{2+} ions, the other metal ions could not induce such an obvious change of the fluorescence spectrum. Therefore, compound **2c** could be used as a highly selective fluorescence quenching probe for Cu^{2+} ions.

Compound **2c** (1×10^{-5} M) was dissolved in HEPES (20 mM, v/v = 8/2, CH_3CH_2OH–H_2O, pH = 7.2) buffer solution with the addition of Cu^{2+} ions (Fig. 4). With the addition of increasing concentrations of Cu^{2+} ions (0–1×10^{-4} M), the fluorescence intensity of compound **2c** gradually weakened until it almost disappeared along with a colour change from blue to colourless.

A linear relationship between the fluorescence intensity of compound **2c** and Cu^{2+} concentration was also obtained. According to the fluorescence intensity at 450 nm, we established a linear quenching relation with increasing Cu^{2+} concentrations from 0 M to 1×10^{-4} M ($y = -61.667x + 774.935$) (Fig. 5), and the fitting constant was up to 0.9949. The limit of detection (LOD) was calculated from the formula LOD = $3\sigma_{bi}/m$, where σ_{bi} is the standard deviation of the blank data, and m is the slope of the intensity reduction before and after quenching *versus* Cu^{2+} concentration (Fig. S4†). The LOD of Cu^{2+} with compound **2c** was 4.0×10^{-8} M. The quenching mechanism could be divided into a static quenching mechanism and a dynamic quenching mechanism; the UV-vis spectra changes at 325 nm indicated that the quenching effect should be attributed to a static quenching mechanism. The Stern–Volmer equation was introduced in the following section as shown in eqn (1) to further explain the static quenching mechanism:

$$\frac{F_0}{F} = 1 + K_s[Cu^{2+}] \quad (1)$$

where F_0 and F respectively represent the fluorescence intensity of compound **2c** in the absence and presence of Cu^{2+} ions, and K_s is the static quenching constant of the Stern–Volmer

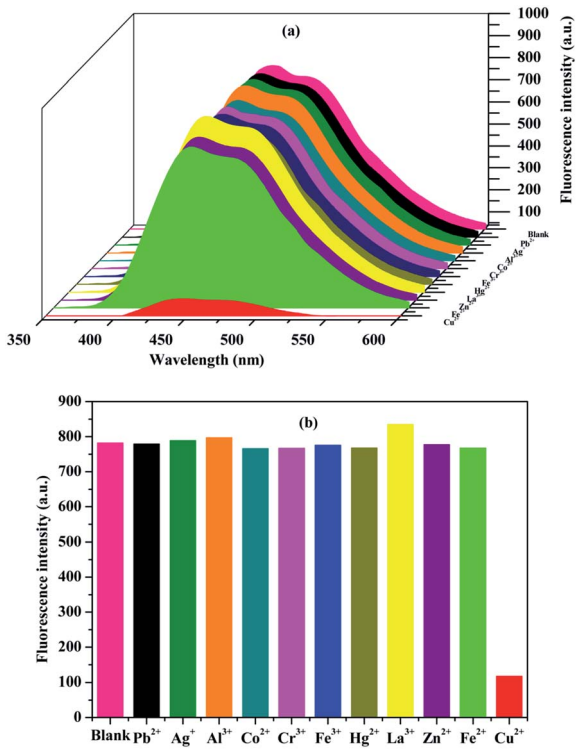

Fig. 3 (a) Fluorescence intensity of compound **2c** (1×10^{-5} M) in response to different metal ions (1×10^{-4} M) in CH_3CH_2OH–H_2O (v/v = 8/2, 20 mM HEPES buffer, pH = 7.2) solution. (b) Fluorescence intensity ($(F_0 - F)/F_0$) of compound **2c** (1×10^{-5} M) at 450 nm in the HEPES buffer solution upon addition of various metal ions. Excitation wavelength of 325 nm; em. slit of 12 nm; ex. slit of 5 nm.

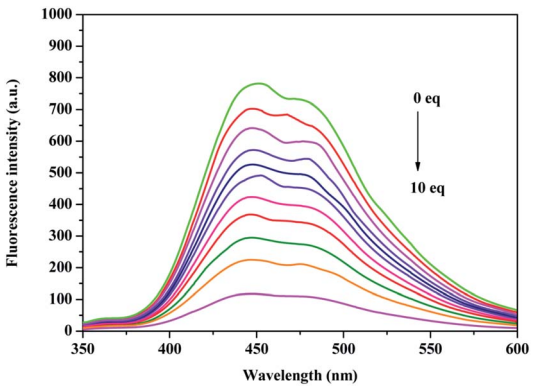

Fig. 4 Fluorescence quenching spectra of compound **2c** (1×10^{-5} M) with increasing concentrations of Cu^{2+} ions in CH_3CH_2OH–H_2O (v/v = 8/2, 20 mM HEPES buffer, pH = 7.2) solution. Excitation wavelength of 325 nm; em. slit of 12 nm; ex. slit of 5 nm.

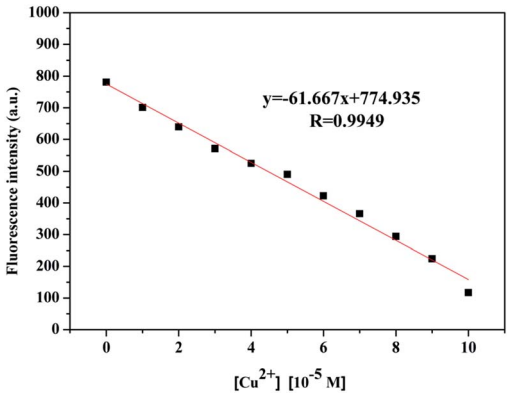

Fig. 5 Fluorescence intensity of compound **2c** (1×10^{-5} M) at 450 nm with increasing concentrations of Cu^{2+} ions in CH_3CH_2OH–H_2O (v/v = 8/2, 20 mM HEPES buffer, pH = 7.2) solution. Excitation wavelength of 325 nm; em. slit of 12 nm; ex. slit of 5 nm.

equation. Based on the linear relation of F_0/F *versus* Cu^{2+} concentration (Fig. S5†), K_s was computed to be 1.21×10^4 L M^{-1}.

The binding stoichiometry between compound **2c** and Cu^{2+} was observed using the rate of intensity change on adjusting the concentration proportions of compound **2c** and Cu^{2+} ions. A Job plot was recorded in 8/2 (v/v) ethanol–water solution (20 mM HEPES, pH = 7.2) (Fig. S6†). The binding stoichiometry of compound **2c** and Cu^{2+} ions was 2 : 1. The ESI-mass spectrum of compound **2c** binding with Cu^{2+} ions also shows a peak at 760.8 *m*/*z*, which was interpreted as $[2 \times \mathbf{2c} + Cu^{2+}\text{–H}]^+$ (Fig. S7†). In addition, the binding constant (K_a) of compound **2c** and Cu^{2+} was evaluated from the intensity titration data using the Benesi–Hildebrand method (eqn (2)):[38]

$$\frac{\alpha^2}{(1-\alpha)} = \frac{1}{2K_a C_F[M]} \quad (2)$$

In eqn (2), C_F is the total concentration of compound **2c** in the system, and α is defined as the ratio between the concentration of free **2c** and the total concentration of compound **2c**. α was obtained using eqn (3):

$$\alpha = \frac{[F - F_0]}{[F_1 - F_0]} \quad (3)$$

where F is the fluorescence intensity of compound **2c** at 450 nm with increasing concentrations of Cu^{2+} ions, and F_1 and F_0 are the fluorescence intensity of free **2c** at 450 nm and the minimal fluorescence intensity of compound **2c** at 450 nm in the presence of Cu^{2+} ions.

The binding constant (K_a) of compound **2c** and Cu^{2+} was obtained according to $\alpha^2/(1-\alpha)$ against $1/[Cu^{2+}]$. The binding constant (K_a) of compound **2c** and Cu^{2+} was calculated to be 1×10^8 M^{-2} (Fig. S8†). In addition, the binding mode of compound **2c** with Cu^{2+} was investigated using IR spectroscopy. As shown in Fig. S9 and S10,† the characteristic stretching band at 3155 cm^{-1}, which corresponds to the amino (ν_{N-H}, NH_2) absorption of compound **2c**, disappeared upon chelation with Cu^{2+}. Moreover, a typical scissor bending peak at 1567 cm^{-1}, which corresponds to the amino (δ_{N-H}, NH_2) absorption of compound **2c**, shifted to a higher frequency (1604 cm^{-1}) in the **2c**–Cu^{2+} complex. The stretching peak corresponding to $\nu_{C=N}$ (pyrimidine) was measured at 1647 cm^{-1} in compound **2c**, while the band strengthened and shifted to a higher frequency (1666 cm^{-1}) in the complex. With significant evidence of characteristic peaks in free **2c** and the complex, the optimized binding mode of **2c** and Cu^{2+} could be concluded on the basis of the above binding study (Fig. S11†).

A performance comparison with some existing Cu^{2+} fluorescence probes is listed in Table S2.† Almost all of the enhanced fluorescence probes or quenched fluorescence probes show excellent selectivity to Cu^{2+} and an extremely low detection limit (μM).[39–46] Fluorescence imaging towards Cu^{2+} has been widely applied in live cells in completed studies, while compound **2c** maintained a good fluorescence intensity until copper ions were injected in the mice. Compound **2c** could be used as a sensitive and specific probe for Cu^{2+}. In addition, the performance of compound **2c** was not inferior to that of other Cu^{2+} fluorescence probes.

Based on the coexistence of various metal ions in soil, rivers, and animals, the interference from other metal ions has to be taken into account. The competition of compound **2c** (1×10^{-5} M) with Cu^{2+} ions (1×10^{-4} M) was examined in the presence of other metal ions (1×10^{-4} M) by recording successive fluorescence intensity changes in CH_3CH_2OH–H_2O (v/v = 8/2, 20 mM HEPES buffer, pH = 7.2) solution. As shown in Fig. 6, the quenching system of compound **2c** towards Cu^{2+} ions showed a very slight growth with the addition of different metal ions (Pb^{2+}, Ag^+, Al^{3+}, Co^{2+}, Cr^{3+}, Fe^{3+}, Hg^{2+}, La^{3+}, Zn^{2+}, and Fe^{2+}) in the presence of Cu^{2+} ions. The detection of Cu^{2+} ions using compound **2c** was not affected by other metal ions. Thus, compound **2c** could serve as a specific probe for Cu^{2+} ions in buffer solution.

The fluorescence intensity of compound **2c** (1×10^{-5} M) in different solvents could be regarded as an important indicator of its applicability; compound **2c** was capable of keeping

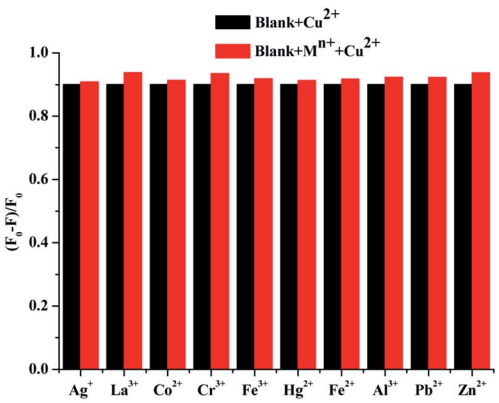

Fig. 6 Fluorescence intensity changes ($(F_0 - F)/F_0$) of compound **2c** (1×10^{-5} M) with Cu^{2+} ions (1×10^{-4} M) in the absence and presence of other metal ions (1×10^{-4} M) in CH_3CH_2OH–H_2O (v/v = 8/2, 20 mM HEPES buffer, pH = 7.2) solution. Excitation wavelength of 325 nm; em. slit of 12 nm; ex. slit of 5 nm.

a relatively higher fluorescence intensity in test solvents (Fig. S12†). The intensity of compound **2c** in DMF was much stronger than that in other solvents, but the intensity was obviously weaker in low-polarity solutions such as methylbenzene and *n*-hexane. When compound **2c** was dissolved in acetonitrile, HEPES buffer solution, 1,4-dioxane, trichloromethane, and ethyl acetate separately, compound **2c** exhibited a moderate fluorescence intensity. In addition, the maximum emission wavelength of compound **2c** showed a tiny red-shift from 435 nm to 450 nm in the test solutions and the fluorescence intensity of compound **2c** had no significant quenching in most of the organic solvents.

Because the fluorescence intensity of compound **2c** could be affected by solvents according to the above research, the fluorescence quenching efficiency of compound **2c** (1×10^{-5} M) to Cu^{2+} ions (1×10^{-4} M) at 450 nm was evaluated in different solvents (Fig. S13†). The fluorescence of compound **2c** was quenched in DMF, acetonitrile, HEPES buffer solution, 1,4-dioxane, trichloromethane, ethyl acetate, methylbenzene, and *n*-hexane in the presence of Cu^{2+} ions. The fluorescence quenching efficiency $(F_0 - F)/F_0$ of compound **2c** reached over 80% in the test solvents, and in particular, the quenching efficiency could reach up to 90% with the addition of Cu^{2+} ions in DMF, acetonitrile, trichloromethane, and ethyl acetate. Compound **2c** could act as a sensitive probe for the determination of Cu^{2+} in different solvents.

We examined the fluorescence properties of compound **2c** (1×10^{-5} M) in the absence and presence of Cu^{2+} ions (1×10^{-4} M) with time. The fluorescence intensity of compound **2c** and the response of compound **2c** towards Cu^{2+} were recorded in HEPES (20 mM, v/v = 8/2, CH_3CH_2OH–H_2O, pH = 7.2) buffer solution (Fig. S14†). With the increase of time from 0 to 3.0 min, the fluorescence intensity of compound **2c** was unchanged in principle. The response time of the probe to the substrate determines whether the substrate could be detected quickly or not; compound **2c** had a very fast response time towards Cu^{2+} in our study. The fluorescence intensity of compound **2c** did not decline after 30 s in the presence of Cu^{2+} ions indicating that the quenching reaction between compound **2c** and Cu^{2+} had been balanced at the moment. The excellent fluorescence stability and the rapid response time towards Cu^{2+} would extend the utilization of compound **2c** in detection.

The fluorescence intensity at 450 nm of compound **2c** (1×10^{-5} M) in the absence and presence of Cu^{2+} ions (1×10^{-4} M) was measured with different pH values (1–13) in 8/2 (v/v) ethanol–water solution (Fig. 7). The fluorescence intensity of compound **2c** was relatively weak in acidic solution and gradually enhanced with increasing pH values until the pH value reached 11. An overly acidic or alkali environment was unfavourable for detecting Cu^{2+} ions; the optimum pH range for compound **2c** to respond to Cu^{2+} ions was between 5 and 11. In view of the wide pH range for detecting Cu^{2+} ions, compound **2c** could be used as a working Cu^{2+} probe for practical application.

To evaluate whether the fluorescence intensity of compound **2c** towards copper ions was affected by the anions of the copper salts, fluorescence curves of compound **2c** with the addition of cupric chloride, cupric bromide, and cupric nitrate were obtained in HEPES (20 mM, v/v = 8/2, CH_3CH_2OH–H_2O, pH = 7.2) buffer solution (Fig. S15†). The quenching intensity showed an obvious difference under the action of the corresponding copper salts, and the optimal fluorescence quenching efficiency of compound **2c** towards copper ions was found in the presence of cupric nitrate. With the addition of Cu^{2+} ions, the fluorescence intensity of compound **2c** was quenched effectively.

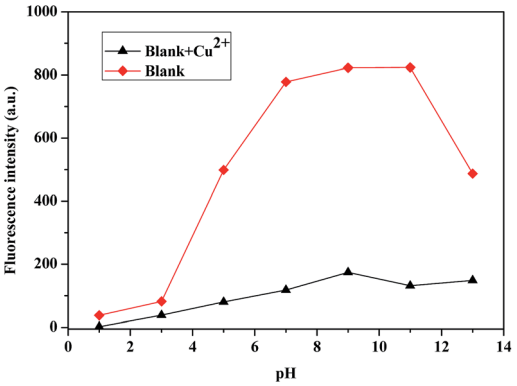

Fig. 7 Fluorescence intensity changes of compound **2c** (1×10^{-5} M) in the absence and presence of Cu^{2+} (1×10^{-4} M) at 450 nm with different pH values. Excitation wavelength of 325 nm; em. slit of 12 nm; ex. slit of 5 nm.

The reversible and reusable response of compound **2c** was investigated by performing four alternate cycles of titration of compound **2c** with Cu^{2+} followed by the addition of EDTA (Fig. S16†). An obvious decrease of the fluorescence intensity resulted from the formation of the **2c**–Cu^{2+} complex. However, the fluorescence intensity of the system returned to a level close to that of the free compound **2c** with the addition of EDTA. The repeated OFF/ON behavior verified the remarkable reversibility and reusability of compound **2c** in detecting Cu^{2+} ions.

The photo-stability of compound **2c** was evaluated upon continuous illumination in HEPES (20 mM, v/v = 8/2, CH_3CH_2-OH–H_2O, pH = 7.2) buffer solution. As shown in Fig. S17,† the fluorescence intensity of compound **2c** at 450 nm showed no significant decrease upon continuous illumination for 60 h with a fluorescent lamp. The excellent photo-stability of compound **2c** indicated that it could be used as a practical fluorescence probe.

The thermostability of compounds 2a–2c

The thermostability is an important parameter for a fluorescence probe to evaluate its applicability. We tested the thermostability of compounds **2a–2c** using TGA (Fig. S18†). All of compounds **2a–2c** had excellent thermostabilities, and the thermostabilities of compounds **2b** and **2c** were much better than that of compound **2a**. The weight loss of compounds **2a–2c** attained 10% at the temperature points approaching 255.3 °C, 277.0 °C, and 275.9 °C. Compared to compound **2a**, compounds **2b** and **2c** had better thermostabilities.

Fluorescence response to various metal ions on filter paper

The detection of a fluorescence probe towards a substrate should ensure accuracy as simply as possible, so we attempted

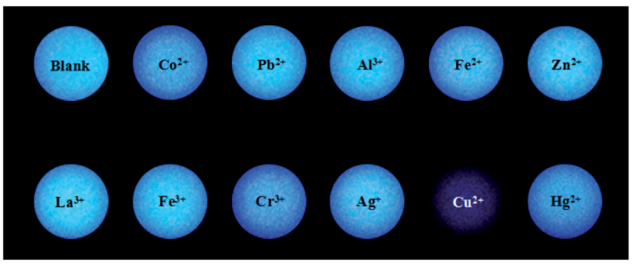

Fig. 8 Fluorescence photographs of compound **2c** (1×10^{-5} M) with drops of various metal ions (1.5×10^{-4} M) on filter paper.

to use compound **2c** to distinguish Cu^{2+} ions from other metal ions on filter paper. The solution of compound **2c** (1×10^{-5} M) was added dropwise and evenly on the filter paper, then water solutions of metal salts (1.5×10^{-4} M) were respectively dropped in the previous circles and dried on the filter paper. As shown in Fig. 8, compound **2c** in the absence or presence of Zn^{2+}, Hg^{2+}, Fe^{2+}, Fe^{3+}, Ag^{+}, Al^{3+}, and Pb^{2+} exhibits a bright fluorescent circle on the filter paper under 365 nm UV light, while the fluorescent circles of compound **2c** were quenched slightly with Co^{2+} and Cr^{3+} ions and enhanced mildly with La^{3+} ions. With the drop of Cu^{2+} ions, the fluorescent circles of compound **2c** changed from bright blue to a dark colour. Compound **2c** could quickly and simply recognize Cu^{2+} ions from other metal ions on filter paper, so it was likely to be a feasible way to detect Cu^{2+} ions.

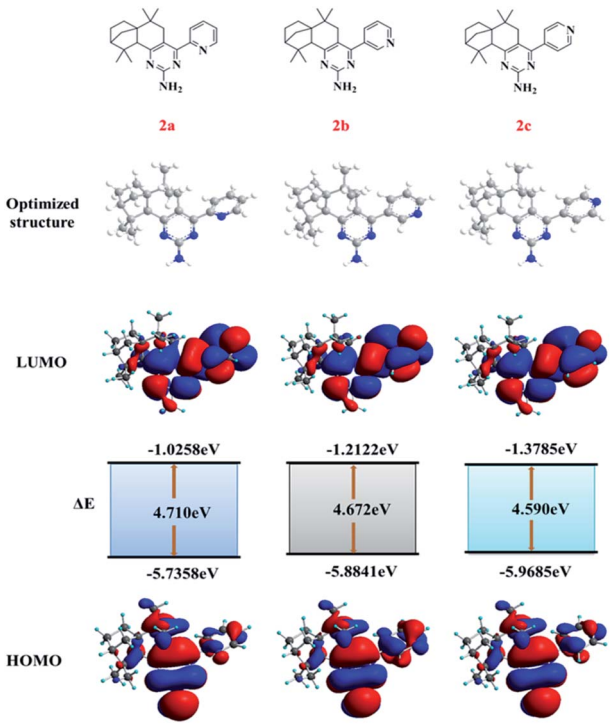

Fig. 9 The optimized structures and molecular orbitals (LUMO and HOMO) of compounds **2a–2c**.

DFT calculations

For further understanding optical properties of synthetic compounds with density functional theory (DFT), the

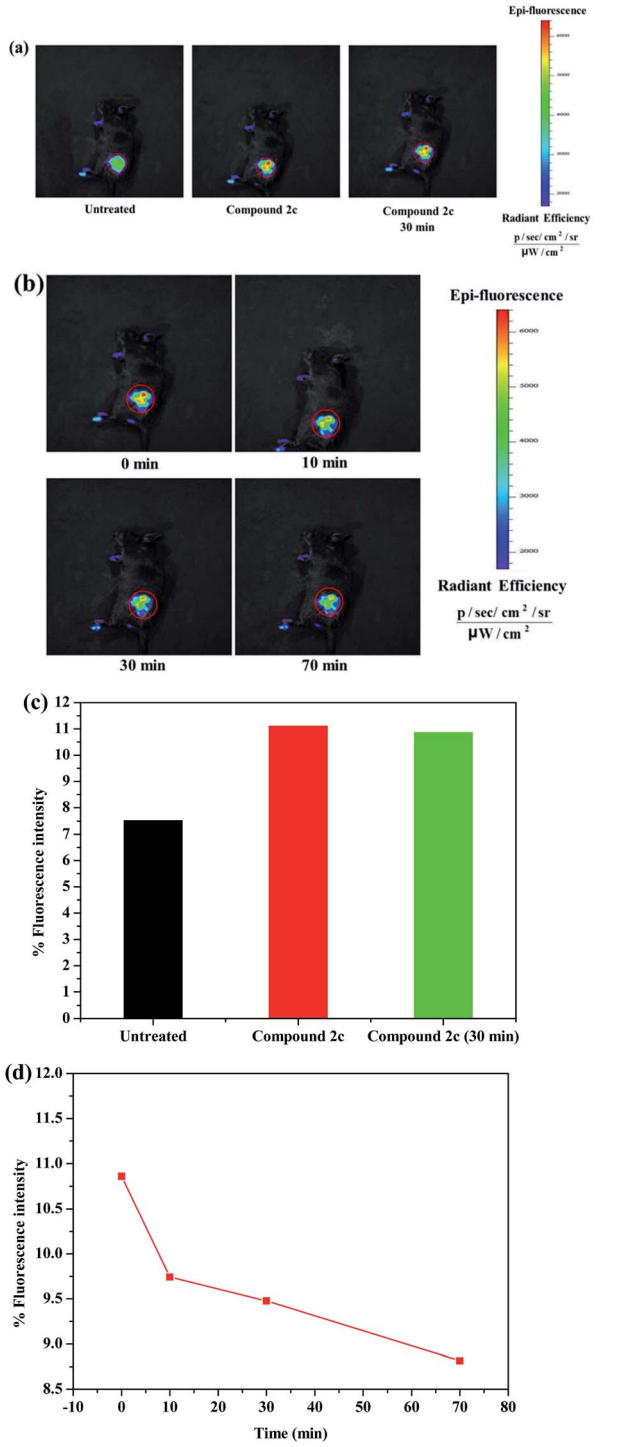

Fig. 10 (a) The fluorescence images of untreated black mice and mice given a skin-pop injection of compound **2c** (50 μl × 20 μM), then incubated for 30 min. (b) The fluorescence images of black mice injected with compound **2c** and 1.5 equivalents Cu^{2+} ions and incubated for 0, 10, 30, and 70 min. (c and d) Quantified fluorescence signals of (a) and (d), respectively.

geometries of compounds **2a–2c** were optimized at the B3LYP level with the 6-31G(d) basis set using the Gaussian 09 program. The optimized structures of compounds **2a–2c** were obtained. In addition, the lowest unoccupied molecular orbital (LUMO) and the highest occupied molecular orbital (HOMO) are also shown in Fig. 9. The HOMOs of compounds **2a–2c** were distributed over the molecules except for the partial isolongifolanone units, while the LUMOs were mainly situated on the pyridine and pyrimidine groups. The HOMO–LUMO band gaps (ΔE) acted as the theoretical basis of the molecular fluorescence properties. The band gaps (ΔE) of compounds **2a–2c** were 4.710 eV, 4.672 eV, and 4.590 eV, and they decreased with the increase of the distance of the nitrogen atoms on the pyridine groups from the pyrimidine units. The lowest ΔE indicated that compound **2c** could show fluorescence after electron transition more easily than the other compounds could.

Bio-imaging *in vivo* of compound 2c

The part around a mouse's hip with loose muscle tissues and abundant blood vessels enables an imaging agent to be absorbed as quickly as possible. Therefore, the fluorescence imaging efficacy of compound **2c** towards copper ions was evaluated *in vivo* in black mice using a near-infrared (NIR) fluorescence imaging system. A solution of compound **2c** (50 μl × 20 μM in saline, containing 1% DMSO) was injected into the subcutaneous tissues on the hip of the black mice. The fluorescence variation at the same region of the black mice was obvious after the injection of compound **2c** (Fig. 10a and S43a†); the florescence intensity in the tissue sharply increased from 7.52 to 11.11% (Fig. 10c). Compared with the initial fluorescence imaging (immediately recorded after compound **2c** was injected), the fluorescence durability of compound **2c** was also investigated within 30 min. As shown in the diagrams, the fluorescence signal after 30 min at the same injecting region had no significant change; the % florescence intensity almost did not weaken during the testing time. The fluorescence imaging of compound **2c** was visualized after the black mice were treated with an injection of 1.5 equivalents Cu^{2+} after 0, 10, 30, and 70 min, and the graphs at the same region show a quenching reaction over time (Fig. 10b and S43b†). The % fluorescence intensity of compound **2c** towards Cu^{2+} ions exhibited a constant decrease in the black mice within the testing time; the quenching velocity of the % fluorescence intensity ($\Delta\%\ F/\Delta t$) was fastest ten minutes before and then mildly slowed down with time (Fig. 10d). Compound **2c** had a good florescence durability and short response time to Cu^{2+} *in vivo*, so it could be used as an excellent probe for imaging Cu^{2+} ions in living black mice.

Conclusions

In summary, a novel fluorescence probe has been synthesized from isolongifolanone. The sensor exhibited highly selective and sensitive fluorescence quenching towards Cu^{2+} ions, and the detection limit for Cu^{2+} ions was 4.0×10^{-8} M. In addition, the quenching constant (1.21×10^{4} L M^{-1}) and the binding constant (1×10^{8} M^{-2}) were also obtained according to the linear relationship between the fluorescence intensity and Cu^{2+} ion concentration. The sensor could detect Cu^{2+} ions in a wide pH range of 5–11 and the detection could be achieved in different solvents. The sensor could respond to Cu^{2+} ions in a short time (0.5 min) and sustain a good quenching efficiency during the testing time. A simple method was provided for detecting Cu^{2+} ions using the sensor on filter paper. The sensor was applied to the detection Cu^{2+} ions in living mice, and the fluorescence signals were quantified to visualize the quenching effect *in vivo*. Moreover, the fluorescence sensor was synthesized from isolongifolanone, which is an important derivative of turpentine. Therefore, the synthesized sensor has exploited the utilization of turpentine and provided a possible route for deep processing of forest resources.

Experimental

Instruments

The mass spectra were recorded on an America Agilent 5975c mass spectrometer. The purity was measured on an America Agilent 7890A gas chromatograph. The ^{13}C NMR and ^{1}H NMR spectra were recorded in DMSO-d_6 or $CDCl_3$ solutions on a Bruker AV 500 spectrometer. The UV-vis absorption spectra were determined on a Shimadzu UV-2450 spectrophotometer. The fluorescence spectra were obtained on a Perkin Elmer LS 55 fluorescence spectrophotometer with the excitation wavelength at 325 nm. The infrared spectra were measured on a Nicolet 380 FTIR infrared spectrometer. The melting points were recorded on an X-6 microscopic melting point apparatus. Single-crystal X-ray diffraction measurements were done on a Bruker D8 Venture area diffractometer. The pH values were collected on a Model PHS-3C pH meter. The fluorescence images of living mice were taken using a Maestro *In Vivo* Imaging System.

Materials

All the reagents and solvents were purchased from various commercial sources and used without further purification. Deionized water was used throughout the experiment. The most common solutions of the sensor were prepared in HEPES buffer solution (20 mM, pH = 7.2, CH_3CH_2OH–H_2O, v/v = 8/2). The variety of pH solutions from 1 to 13 were prepared using HCl and NaOH solutions at a concentration of 1 M for slight pH adjustments. The stock solutions of metal ions were prepared from various metal salts ($ZnCl_2$, $HgSO_4$, $Fe(NO_3)_3 \cdot 9H_2O$, $FeCl_2$, $CuCl_2 \cdot H_2O$, $CrCl_3 \cdot 6H_2O$, $Co(NO_3)_2 \cdot 6H_2O$, $La(NO_3)_3 \cdot 6H_2O$, $AgNO_3$, $AlCl_3$, $Pb(NO_3)_2$, $CuBr_2$, and $Cu(NO_3)_2 \cdot 3H_2O$). The sensor used in the mice was dissolved in saline (containing 1% DMSO) and the $CuCl_2 \cdot H_2O$ used in the mice was dissolved in saline.

Methods

All experiments involving living animals and their care were performed in strict accordance with the National Care and Use of Laboratory Animals by the National Animal Research Authority (China) and guidelines of Animal Care and Use issued

by the Medical School of Southeast University Institutional Animal Care and Use Committee, and the experiments were approved by the Institutional Animal Care and Use Committee of the Medical School of Southeast University.

Synthesis of 7-(pyridine-2′-ylmethylene)-isolongifolanone (1a). Isolongifolanone (2.2 g, 8 mmol), *tert*-butyl alcohol (30 mL), potassium *tert*-butoxide (0.84 g, 7.5 mmol), and pyridine-2-carboxaldehyde (1.07 g, 10 mmol) were successively added in a 50 mL dried three-necked flask equipped with a stirrer, condenser, and thermometer. The mixture was stirred and refluxed for 4 h until the conversion ratio of isolongifolanone exceeded 95% (monitored by GC). The reacted solution was evaporated under vacuum and extracted three times with 20 mL ethyl acetate, then the merged organic layers were washed to neutrality with saturated salt water, dried with sodium sulfate, filtered, and evaporated to afford a crude product, then recrystallized with ethanol in a refrigerator. Pale yellow crystals were afforded (67.5% yield). Mp: 102.5–102.6 °C; FT-IR (KBr, cm^{-1}) ν: 2964, 2871, 1670, 1600, 1471, 1426, 1385, 1238, 1198, 1176, 921, 816, 736; ^{1}H NMR (400 MHz, $CDCl_3$, ppm) δ: 0.85 (s, 2H), 1.06 (s, 3H), 1.09–1.16 (m, 1H), 1.22 (s, 3H), 1.26–1.30 (m, 1H), 1.45–1.53 (m, 1H), 1.61–1.68 (m, 1H), 1.74 (d, J = 4 Hz), 1.80–1.83 (m, 2H), 1.99 (s, 1H), 2.97–3.02 (m, 1H), 3.10–3.15 (m, 1H), 7.15 (t, J = 4 Hz, 1H), 7.39 (d, J = 4 Hz, 2H), 7.66 (t, J = 8 Hz, 1H), 8.67 (d, J = 4 Hz, 1H); ^{13}C NMR (100 MHz, $CDCl_3$, ppm) δ: 24.13, 24.48, 25.27, 25.43, 28.14, 30.05, 31.14, 37.45, 41.62, 44.62, 47.88, 55.49, 62.89, 122.07, 126.92, 133.40, 135.85, 139.36, 149.28, 155.39, 203.35; EIMS m/z (%): 309 (M^+, 100), 294 (56), 281 (19), 266 (26), 252 (7), 200 (45), 131 (73), 93 (68); HRMS (m/z): $[M + H]^+$ calcd for $C_{21}H_{27}NO + H^+$, 310.2171; found, 310.2178.

Synthesis of 6,6,10,10-tetramethyl-4-(pyridine-2′-yl)-5,7,8,9,10,10*a*-hexahydro-6*H*-6*a*,9-methanobenzo[*h*]quinazolin-2-amine (2a). 7-(Pyridine-2′-ylmethylene)-isolongifolanone (1.54 g, 5 mmol), guanidine hydrochloride (1.91 g, 20 mmol), *tert*-butyl alcohol (60 mL), and *tert*-butoxide (2.8 g, 25 mmol) were successively added in a 100 mL dried three-necked flask equipped with a stirrer, condenser, and thermometer. The mixture was stirred and refluxed for 18 h until the conversion ratio of 7-(pyridine-2′-ylmethylene)-isolongifolanone was over 95% (monitored by GC). The reacted mixture was evaporated under vacuum and extracted three times with ethyl acetate, then the combined organic layers were washed to neutrality with saturated brine, dried with sodium sulfate, filtered, and evaporated to afford a viscous liquid, then recrystallized with ethanol and ethyl acetate in a refrigerator. The final product was a white powder (35.0%, yield). Mp: 176.8–177.1 °C; FT-IR (KBr, cm^{-1}) ν: 3489, 3265, 3139, 2959, 2934, 2869, 1618, 1552, 1458, 1408, 1372, 1209, 992, 797; ^{1}H NMR (300 MHz, DMSO-d_6, ppm) δ: 0.61 (s, 3H), 0.72 (s, 3H), 0.91 (s, 3H), 1.06–1.09 (m, 1H), 1.17 (d, J = 9 Hz, 1H), 1.32 (s, 3H), 1.46–1.50 (m, 2H, 1H), 1.59 (d, J = 12 Hz, 1H), 1.69 (s, 2H), 1.82 (s, 1H), 2.21–2.29 (m, 2H), 2.79 (d, J = 15 Hz, 1H), 3.34 (s, 1H), 6.19 (s, 2H), 7.41 (t, J = 6 Hz, 1H), 7.78 (d, J = 6 Hz, 1H), 7.89 (t, J = 6 Hz, 1H), 8.63 (d, J = 3 Hz, 1H); ^{13}C NMR (75 MHz, DMSO-d_6, ppm) δ: 22.88, 24.32, 25.20, 25.52, 28.06, 29.68, 31.74, 36.69, 38.64, 43.67, 47.41, 54.57, 57.10, 114.66, 123.36, 123.31, 136.49, 148.05, 157.17, 160.68, 162.72, 168.81; EIMS m/z (%): 348 (M^+, 37), 333 (100), 250 (4), 239 (2), 105 (1), 78 (2); HRMS (m/z): $[M + H]^+$ calcd for $C_{22}H_{28}N_4 + H^+$, 349.2392; found, 349.2402.

Synthesis of 7-(pyridine-3′-ylmethylene)-isolongifolanone (1b). Isolongifolanone (2.2 g, 8 mmol), *tert*-butyl alcohol (30 mL), potassium *tert*-butoxide (0.84 g, 7.5 mmol), and pyridine-3-carboxaldehyde (1.07 g, 10 mmol) were successively added in a 50 mL dried three-necked flask equipped with a stirrer, condenser, and thermometer. The mixture was stirred and refluxed for 5 h until the conversion ratio of isolongifolanone exceeded 95% (monitored by GC). The reacted solution was evaporated under vacuum and extracted three times with 20 mL ethyl acetate, then the merged organic layers were washed to neutrality with saturated salt water, dried with sodium sulfate, filtered, and evaporated to afford a crude product, then recrystallized with ethanol in a refrigerator. Pale yellow crystals were afforded (66.8%, yield). Mp: 73.5–73.7 °C; FT-IR (KBr, cm^{-1}) ν: 2964, 2873, 1674, 1597, 1468, 1412, 1367, 1237, 1180, 960, 816, 707; ^{1}H NMR (400 MHz, $CDCl_3$, ppm) δ: 0.83 (s, 3H), 0.85 (s, 3H), 0.92–0.95 (m, 1H), 1.03 (s, 3H), 1.21 (s, 3H), 1.29 (d, J = 4 Hz, 1H), 1.48–1.54 (m, 1H), 1.60–1.67 (m, 1H), 1.76–1.83 (m, 3H), 1.97 (d, J = 4 Hz), 2.52–2.57 (m, 1H) 2.81–2.86 (m, 1H), 7.31–7.34 (m, 1H), 7.44 (s, 1H), 7.75 (d, J = 4 Hz, 1H), 8.51–8.53 (m, 1H), 8.69 (d, J = 4 Hz, 1H); ^{13}C NMR (100 MHz, $CDCl_3$, ppm) δ: 24.28, 24.78, 25.67, 25.79, 28.45, 30.43, 31.90, 37.78, 41.80, 45.03, 48.21, 55.70, 63.09, 123.52, 132.05, 132.74, 137.47, 137.67, 148.96, 151.23, 202.35; EIMS m/z (%): 309 (M^+, 71), 294 (27), 280 (24), 266 (100), 252 (32), 240 (37), 117 (54), 93 (24); HRMS (m/z): $[M + H]^+$ calcd for $C_{21}H_{27}NO + H^+$, 310.2171; found, 310.2177.

Synthesis of 6,6,10,10-tetramethyl-4-(pyridine-3′-yl)-5,7,8,9,10,10*a*-hexahydro-6*H*-6*a*,9-methanobenzo[*h*]quinazolin-2-amine (2b). 7-(Pyridine-3′-ylmethylene)-isolongifolanone (1.54 g, 5 mmol), guanidine hydrochloride (1.91 g, 20 mmol), *tert*-butyl alcohol (60 mL), and *tert*-butoxide (2.8 g, 25 mmol) were successively added in a 100 mL dried three-necked flask equipped with a stirrer, condenser, and thermometer. The mixture was stirred and refluxed for 20 h until the conversion ratio of 7-(pyridine-3′-ylmethylene)-isolongifolanone was over 95% (monitored by GC). The reacted mixture was evaporated under vacuum and extracted three times with ethyl acetate, then the combined organic layers were washed to neutrality with saturated brine, dried with sodium sulfate, filtered, and evaporated to afford a viscous liquid, then recrystallized with ethanol and ethyl acetate in a refrigerator. The final product was a white powder (33.2%, yield). Mp: 245.3–245.7 °C; FT-IR (KBr, cm^{-1}) ν: 3482, 3281, 3157, 2961, 2870, 1618, 1552, 1455, 1400, 1375, 1210, 1024, 797; ^{1}H NMR (400 MHz, DMSO-d_6, ppm) δ: 0.59 (s, 3H), 0.75 (s, 3H), 0.93 (s, 3H), 1.05 (d, J = 4 Hz, 1H), 1.15–1.19 (m, 1H), 1.31 (s, 3H), 1.47–1.52 (m, 1H), 1.55–1.64 (m, 2H), 1.70 (d, J = 4 Hz, 1H), 1.78–1.86 (m, 1H), 1.98 (d, J = 16 Hz, 1H), 2.19 (s, 1H), 2.84 (d, J = 16 Hz, 1H), 6.26 (s, 2H), 7.46–7.49 (m, 1H), 7.95–7.98 (m, 1H), 8.61 (d, J = 4 Hz, 1H), 8.74 (d, J = 4 Hz, 1H); ^{13}C NMR (75 MHz, DMSO-d_6, ppm) δ: 23.45, 24.06, 25.04, 25.79, 26.23, 28.74, 30.36, 32.86, 37.42, 39.39, 44.41, 48.04, 55.42, 57.82, 114.91, 123.69, 134.88, 137.00, 150.13, 161.63, 162.95, 169.38; EIMS m/z (%): 348 (M^+, 100), 333 (26), 319 (32), 266 (88), 251 (20), 237 (12), 105 (8), 78

(7); HRMS (*m*/*z*): $[M + H]^+$ calcd for $C_{22}H_{28}N_4 + H^+$, 349.2392; found, 349.2409.

Synthesis of 7-(pyridine-4′-ylmethylene)-isolongifolanone (1c). Isolongifolanone (2.2 g, 8 mmol), *tert*-butyl alcohol (30 mL), potassium *tert*-butoxide (0.84 g, 7.5 mmol), and pyridine-4-carboxaldehyde (1.07 g, 10 mmol) were successively added in a 50 mL dried three-necked flask equipped with a stirrer, condenser, and thermometer. The mixture was stirred and refluxed for 5 h until the conversion ratio of isolongifolanone exceeded 95% (monitored by GC). The reacted solution was evaporated under vacuum and extracted three times with 20 mL ethyl acetate, then the merged organic layers were washed to neutrality with saturated salt water, dried with sodium sulfate, filtered, and evaporated to afford a crude product, then recrystallized with ethanol in a refrigerator. Pale yellow crystals were afforded (64.2%, yield). Mp: 88.5–88.6 °C; FT-IR (KBr, cm^{-1}) *ν*: 2965, 2933, 2874, 1672, 1588, 1467, 1411, 1364, 1233, 1186, 957, 814, 787; ^{1}H NMR (400 MHz, $CDCl_3$, ppm) *δ*: 0.85 (s, 3H), 0.87 (s, 3H), 0.95–1.01 (m, 1H), 1.06 (s, 3H), 1.24 (s, 3H), 1.32 (d, $J = 4$ Hz, 1H), 1.50–1.57 (m, 1H), 1.63–1.70 (m, 1H), 1.79–1.88 (m, 3H), 2.00 (d, $J = 4$ Hz, 1H), 2.56 (d, $J = 16$ Hz, 1H), 2.82–2.87 (m, 1H), 7.30 (d, $J = 8$ Hz, 2H), 7.39 (s, 1H), 8.63 (d, $J = 8$ Hz, 2H); ^{13}C NMR (100 MHz, $CDCl_3$, ppm) *δ*: 23.99, 24.49, 25.40, 25.49, 28.13, 30.19, 31.59, 37.52, 41.33, 44.80, 47.95, 55.46, 62.88, 124.10, 133.12, 134.25, 139.16, 143.30, 149.73, 149.95, 202.04; EIMS *m*/*z* (%): 309 (M^+, 100), 294 (52), 280 (12), 266 (37), 252 (63), 238 (50), 135 (37), 93 (63); HRMS (*m*/*z*): $[M + H]^+$ calcd for $C_{21}H_{27}NO + H^+$, 310.2171; found, 310.2171.

Synthesis of 6,6,10,10-tetramethyl-4-(pyridine-4′-yl)-5,7,8,9,10,10*a*-hexahydro-6*H*-6*a*,9-methanobenzo[*h*]quinazolin-2-amine (2c). 7-(Pyridine-4′-ylmethylene)-isolongifolanone (1.54 g, 5 mmol), guanidine hydrochloride (1.91 g, 20 mmol), *tert*-butyl alcohol (60 mL), and *tert*-butoxide (2.8 g, 25 mmol) were successively added in a 100 mL dried three-necked flask equipped with a stirrer, condenser, and thermometer. The mixture was stirred and refluxed for 18 h until the conversion ratio of 7-(pyridine-4′-ylmethylene)-isolongifolanone was over 95% (monitored by GC). The reacted mixture was evaporated under vacuum and extracted three times with ethyl acetate, then the combined organic layers were washed to neutrality with saturated brine, dried with sodium sulfate, filtered, and evaporated to afford a viscous liquid, then recrystallized with ethanol and ethyl acetate in a refrigerator. The final product was a white powder (33.2%, yield). Mp: 272.2–272.4 °C; FT-IR (KBr, cm^{-1}) *ν*: 3327, 3156, 2960, 2925, 2872, 1647, 1567, 1544, 1465, 1407, 1386, 1213, 998, 825, 793; ^{1}H NMR (400 MHz, $CDCl_3$, ppm) *δ*: 0.65 (s, 3H), 0.77 (s, 3H), 0.97 (s, 3H), 1.12 (s, 1H), 1.24 (s, 3H), 1.36 (s, 3H), 1.49–1.56 (m, 1H), 1.61–1.65 (m, 1H), 1.71 (d, $J = 8$ Hz, 1H), 1.76 (s, 1H), 1.90 (t, $J = 8$ Hz, 1H), 2.07–2.13 (m, 1H), 2.31 (s, 1H), 2.69 (d, $J = 16$ Hz, 1H), 4.98 (s, 2H), 7.42 (d, $J = 4$ Hz, 2H), 8.70 (d, $J = 8$ Hz, 2H); ^{13}C NMR (100 MHz, $CDCl_3$, ppm) *δ*: 23.16, 24.34, 24.95, 25.59, 26.10, 28.56, 29.88, 30.33, 32.86, 37.46, 39.32, 44.63, 48.20, 55.45, 58.13, 116.38, 123.59, 146.56, 150.04, 160.65, 163.57, 170.86; EIMS *m*/*z* (%): 348 (M^+, 100), 333 (17), 319 (30), 266 (76), 251 (14), 237 (10), 105 (7), 78 (6); HRMS (*m*/*z*): $[M + H]^+$ calcd for $C_{22}H_{28}N_4 + H^+$, 349.2392; found, 349.2393.

Acknowledgements

The research was support by the Doctorate Fellowship Foundation of Nanjing Forestry University, the University Science Research Project of Jiangsu Province (No. 14KJ220001), the Natural National Science Foundation of China (No. 31470592), the Open Funding of Jiangsu Key Laboratory of Biomass Energy and Materials (No. JSBEM2014010), the Specialized Research Fund for the Doctoral Program of Higher Education of China (163030106), and the key technology of green processing and efficient utilization on Oleoresin (No. 2016YFD0600804).

Notes and references

1 L. Huang, F. Hou, J. Cheng, P. Xi, F. Chen, D. Bai and Z. Zeng, *Org. Biomol. Chem.*, 2012, **10**, 9634–9638.
2 D. Huang, Z. Gao, H. Yi, Y. Bing, C. G. Niu, Q. Guo and C. Lai, *Anal. Methods*, 2014, **7**, 353–358.
3 S. Y. Jiao, K. Li, W. Zhang, Y. H. Liu, Z. Huang and X. Q. Yu, *Dalton Trans.*, 2014, **44**, 1358–1365.
4 T. Anand, G. Sivaraman, A. Mahesh and D. Chellappa, *Anal. Chim. Acta*, 2014, **853**, 596–601.
5 Y. Zhou, H. Zhou, J. Zhang, L. Zhang and J. Niu, *Spectrochim. Acta, Part A*, 2012, **98**, 14–17.
6 Y. G. Gao, Q. Tang, Y. D. Shi, Y. Zhang and Z. L. Lu, *Talanta*, 2016, **152**, 438–446.
7 G. He, Q. Meng, X. Zhao, C. He, P. Zhou and C. Duan, *Inorg. Chem. Commun.*, 2016, **65**, 28–31.
8 S. Erdemir and O. Kocyigit, *Talanta*, 2016, **158**, 63–69.
9 H. Gao, S. Chen, X. Rao, S. Shang and Z. Song, *Bioorg. Med. Chem. Lett.*, 2013, **23**, 2254–2259.
10 J. A. Cotruvo Jr, A. T. Aron, K. M. Ramostorres and C. J. Chang, *Chem. Soc. Rev.*, 2015, **44**, 4400–4414.
11 D. J. Waggoner, T. B. Bartnikas and J. D. Gitlin, *Neurobiol. Dis.*, 1999, **6**, 221–230.
12 E. Gaggelli, H. Kozlowski, D. Valensin and G. Valensin, *ChemInform*, 2006, **37**, 1995–2044.
13 K. J. Barnham, C. L. Masters and A. I. Bush, *Nat. Rev. Drug Discovery*, 2004, **3**, 205–214.
14 G. Multhaup, A. Schlicksupp, L. Hesse, D. Beher, T. Ruppert, C. L. Masters and K. Beyreuther, *Science*, 1996, **271**, 1406–1409.
15 D. R. Brown, *Brain Res. Bull.*, 2001, **55**, 165–173.
16 L. D. Rollmann and R. T. Iwamoto, *J. Am. Chem. Soc.*, 1968, **90**, 1455–1463.
17 M. Bernabé-Pineda, M. T. Ramírez-Silva, M. A. Romero-Romo, E. González-Vergara and A. Rojas-Hernández, *Spectrochim. Acta, Part A*, 2004, **60**, 1105–1113.
18 P. Pathirathna, Y. Yang, K. Forzley, S. P. McElmurry and P. Hashemi, *Anal. Chem.*, 2012, **84**, 6298–6302.
19 A. Gonzales, M. Firmino, C. Nomura, F. Rocha, P. Oliveira and I. Gaubeur, *Anal. Chim. Acta*, 2009, **636**, 198–204.
20 Y. Liu, J. Hu, Q. Teng and H. Zhang, *Sens. Actuators, B*, 2017, **238**, 166–174.

21 B. Gu, L. Huang, W. Su, X. Duan, H. Li and S. Yao, *Anal. Chim. Acta*, 2016, **954**, 97–104.
22 K. Ghosh and D. Kar, *J. Inclusion Phenom. Macrocyclic Chem.*, 2013, **77**, 67–74.
23 D. Y. Lee, N. Singh and D. O. Jang, *Tetrahedron Lett.*, 2010, **51**, 1103–1106.
24 Y.-S. Wu, C.-Y. Li, Y.-F. Li, D. Li and Z. Li, *Sens. Actuators, B*, 2016, **222**, 1226–1232.
25 S.-P. Wu, T.-H. Wang and S.-R. Liu, *Tetrahedron*, 2010, **66**, 9655–9658.
26 X. Xue, H. Fang, H. Chen, C. Zhang, C. Zhu, Y. Bai, W. He and Z. Guo, *Dyes Pigm.*, 2016, **130**, 116–121.
27 Y. Li, H. Zhou, S. Yin, H. Jiang, N. Niu, H. Huang, S. A. Shahzad and C. Yu, *Sens. Actuators, B*, 2016, **235**, 33–38.
28 N. R. Chereddy and S. Thennarasu, *Dyes Pigm.*, 2011, **91**, 378–382.
29 Y. Jiang, R. Shen, G. Wei, Y. Cheng and B. Wang, *Tetrahedron*, 2016, **72**, 2354–2358.
30 Y. Hu, J. Zhang, Y.-Z. Lv, X.-H. Huang and S.-l. Hu, *Spectrochim. Acta, Part A*, 2016, **157**, 164–169.
31 C. Li, K. Xiang, Y. Liu, Y. Zheng, B. Tian and J. Zhang, *Res. Chem. Intermed.*, 2015, **41**, 10169–10180.
32 E. Bolygo and N. C. Atreya, *Fresenius. J. Anal. Chem.*, 1991, **339**, 423–430.
33 D. Hocková, A. n. Holý, M. Masojídková and I. Votruba, *Tetrahedron*, 2004, **60**, 4983–4987.
34 Y.-X. Li, Y.-P. Luo, Z. Xi, C. Niu, Y.-Z. He and G.-F. Yang, *J. Agric. Food Chem.*, 2006, **54**, 9135–9139.
35 U. R. Nayak and S. Dev, *Tetrahedron*, 1960, **8**, 42–48.
36 J. Yadav, U. Nayak and S. Dev, *Tetrahedron*, 1980, **36**, 309–315.
37 R. Jian, Y. Jianlai, H. Jianfeng, W. Jiayu, X. Xu, X. Haijun and W. Shifa, *Chin. J. Inorg. Chem.*, 2016, **36**, 2183–2190.
38 V. S. Jisha, A. J. Thomas and D. Ramaiah, *J. Org. Chem.*, 2009, **74**, 6667–6673.
39 J. Wang, H. Li, L. Long, G. Xiao and D. Xie, *J. Lumin.*, 2012, **132**, 2456–2461.
40 X. Wu, X. Gong, W. Dong, J. Ma, J. Chao, C. Li, L. Wang and C. Dong, *RSC Adv.*, 2016, **6**, 59677–59683.
41 X. Yao, Y.-Y. Guo, J.-X. Ru, C. Xu, Y.-M. Liu, W.-W. Qin, G.-L. Zhang, X.-L. Tang and W.-S. Liu, *Sens. Actuators, B*, 2014, **198**, 20–25.
42 H.-F. Wang and S.-P. Wu, *Sens. Actuators, B*, 2013, **181**, 743–748.
43 H. S. Jung, P. S. Kwon, J. W. Lee, J. I. Kim, C. S. Hong, J. W. Kim, S. Yan, J. Y. Lee, J. H. Lee and T. Joo, *J. Am. Chem. Soc.*, 2009, **131**, 2008–2012.
44 Y. Zhang, X. Guo, X. Tian, A. Liu and L. Jia, *Sens. Actuators, B*, 2015, **218**, 37–41.
45 C. Gao, X. Liu, X. Jin, J. Wu, Y. Xie, W. Liu, X. Yao and Y. Tang, *Sens. Actuators, B*, 2013, **185**, 125–131.
46 L. Qu, C. Yin, F. Huo, J. Chao, Y. Zhang and F. Cheng, *Sens. Actuators, B*, 2014, **191**, 158–164.